Tellus (1992), *44A*, 67–78

Barocoupling of the atmosphere and ocean

By JOHN A. T. BYE, *School of Earth Sciences, The Flinders University of South Australia, GPO Box 2100, Adelaide, South Australia 5001, Australia*

(Manuscript received 17 December 1990; in final form 20 August 1991)

ABSTRACT

A stability analysis for a two-layer system with a high density contrast is presented, and applied to a simple model of the coupled ocean-atmosphere which consists of a barotropic atmosphere above an oceanic mixed layer of variable depth. Instability (which we call "barocoupling"), in which a topographic mixed layer Rossby wave is coupled with a divergent barotropic Rossby wave in the atmosphere steered by the wind velocity, occurs for westerly winds above a mixed layer whose depth shallows towards the equator. For the most unstable wave, typical *e*-folding times are 75 days. Oceanic data indicate that mixed layer depth variability is consistent with a barocoupling response. The implications are that weather patterns have a seasonal memory which results from mixed layer-atmospheric interactions of a few months earlier, particularly in the maritime environment of the southern hemisphere. The significance of barocoupling could be tested using a general circulation model which correctly represents mixed layer dynamics.

1. Introduction

The basic global two-layer fluid system is the ocean and atmosphere, and the distinguishing feature of the World climate is its gentle moderation. This quality is expressed by a broad band response with a variability on time scales well separated from the principal annual and diurnal forcing signals.

Much attention has been focussed on time scales which are a few times the diurnal scale (synoptic variability) in the theory of the development of extratropical cyclones and, in recent years, strenuous efforts have been made to appreciate changes on time scales which are a few times the annual scale.

There is arguably however a lack of understanding of the behaviour in the two period ranges which lie respectively between about one week and one year, and between a decade and a century. In these ranges, teleconnection analysis is often used as an aid to prediction or, alternatively, special geographical circumstances are invoked.

It would be much more satisfying if general dynamic processes could be identified which provide the basic variability in these ranges. The application of the dynamics to a general circulation model would then yield a better appreciation of what broad band weather events we can expect. We discuss below the dynamics of the first range occurring on time scales between one week and one year.

One of the players in the action obviously is the ocean but since a much greater homogeneity of conditions exists at the ocean surface than over the land surface, one would expect that a lack of detailed oceanic coverage should only marginally degrade the ability of the weather forecaster to issue long term forecasts. Observations indicate however that this conclusion is false. There is a subtlety of interaction which has not been taken into account, and which has its maximum effect in the oceans of the Southern Hemisphere connected by the southern ocean.

We present a two layer instability analysis for a system of high density contrast which when applied to the air-sea system, moderates events in the first period range. The term "barocoupling" has been used to emphasize that shearing stresses and heat exchange are not involved in the mechanism, in which the potential energy of the air-sea system is converted into a growing Rossby wave common to both fluids. The existence of a barotropic atmosphere, and an oceanic mixed layer (produced by thermodynamic processes associated with the coupled system) are the only necessary entities.

2. The two-layer system

The formulation of the problem is similar to that by Pedlosky (1964) for the atmosphere, and by Gill et al. (1974) for the ocean. We retain however a general density difference, applicable to either a low density contrast or a high density contrast situation, and express the flowfield in terms of a mass streamfunction, rather than a volume streamfunction.

The equations of motion for the upper layer are,

$$\frac{\partial u_1}{\partial t}+u_1\frac{\partial u_1}{\partial x}+v_1\frac{\partial u_1}{\partial y}-fv_1=-g\frac{\partial \eta_1}{\partial x},$$

$$\frac{\partial v_1}{\partial t}+u_1\frac{\partial v_1}{\partial x}+v_1\frac{\partial v_1}{\partial y}+fu_1=-g\frac{\partial \eta_1}{\partial y}, \tag{1}$$

and for the lower layer are,

$$\frac{\partial u_2}{\partial t}+u_2\frac{\partial u_2}{\partial x}+v_2\frac{\partial u_2}{\partial y}-fv_2 =-\left(\frac{\rho_2-\rho_1}{\rho_2}\right)g\frac{\partial \eta_2}{\partial x}-\frac{\rho_1}{\rho_2}g\frac{\partial \eta_1}{\partial x},$$

$$\frac{\partial v_2}{\partial t}+u_2\frac{\partial v_2}{\partial x}+v_2\frac{\partial v_2}{\partial y}+fu_2 =-\left(\frac{\rho_2-\rho_1}{\rho_2}\right)g\frac{\partial \eta_2}{\partial y}-\frac{\rho_1}{\rho_2}g\frac{\partial \eta_1}{\partial y}, \tag{2}$$

where Ox is towards the east, and Oy is towards the north, and u_1 and u_2 are respectively the horizontal velocity in the upper layer ($\alpha=1$) and the lower layer ($\alpha=2$). ρ_1 and ρ_2 are respectively the density, and η_1 and η_2 the displacement of the upper surface, of each layer, and g is the acceleration of gravity, and $f=2\Omega\sin\theta$ is the Coriolis parameter in which Ω is the angular rotation of the Earth, and θ is latitude (Fig. 1).

From eqs. (1) and (2), we derive the vorticity equations,

$$\left(\frac{\partial}{\partial t}+u_\alpha\frac{\partial}{\partial x}+v_\alpha\frac{\partial}{\partial y}\right)\left(\frac{\zeta_\alpha+f}{h_\alpha}\right)=0, \quad \alpha=1,2, \tag{3}$$

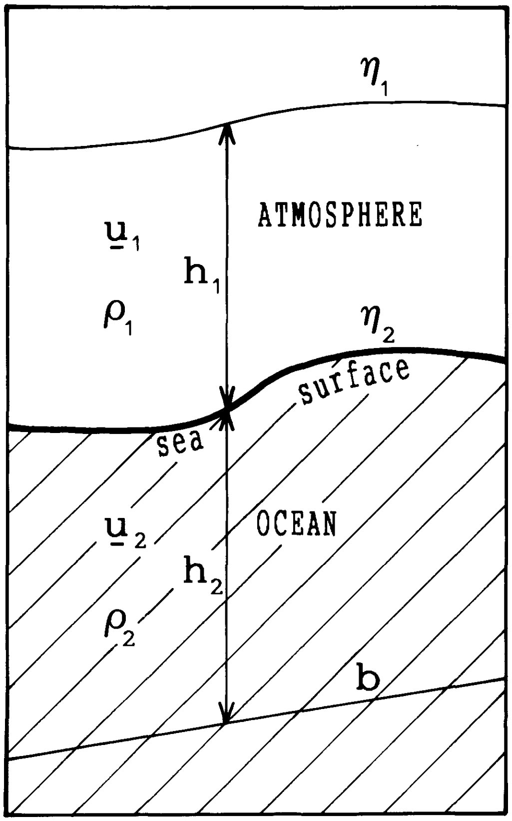

Fig. 1. The two-layer atmosphere-ocean model.

where h_α are the depths, and

$$\zeta_\alpha=\frac{\partial v_\alpha}{\partial x}-\frac{\partial u_\alpha}{\partial y}, \qquad \alpha=1,2$$

are the local vorticities of each layer.

On assuming a β-plane expansion in which

$$f=f_0+\beta y$$

and f_0 and β are constants, and expanding the operands in a Rossby number ($R_0=U_0/f_0L$) expansion where U_0 and L are respectively characteristic horizontal velocity and length scales and $R_0\ll 1$ (Pedlosky, 1964), eq. (3) yields

$$\left(\frac{\partial}{\partial t}+u_1\frac{\partial}{\partial x}+v_1\frac{\partial}{\partial y}\right)\left(\frac{\beta}{f_0}y+\frac{\zeta_1}{f_0}-\frac{\eta_1}{H_1}+\frac{\eta_2}{H_1}\right)=0,$$

$$\left(\frac{\partial}{\partial t}+u_2\frac{\partial}{\partial x}+v_2\frac{\partial}{\partial y}\right)\left(\frac{\beta}{f_0}y+\frac{b}{H_2}+\frac{\zeta_2}{f_0}-\frac{\eta_2}{H_2}\right)=0, \tag{4}$$

where $h_1 = H_1 + \eta_1 - \eta_2$, and $h_2 = H_2 + \eta_2 - b$, in which H_1 and H_2 are the reference depths of each layer and b is the negative depth anomaly. Finally, on defining the geostrophic mass streamfunctions,

$$\rho_1 v_1 = \frac{\partial \Psi_1}{\partial x}, \qquad \rho_1 u_1 = -\frac{\partial \Psi_1}{\partial y},$$

$$\rho_2 v_2 = \frac{\partial \Psi_2}{\partial x}, \qquad \rho_2 u_2 = -\frac{\partial \Psi_2}{\partial y}, \tag{5}$$

and approximating the convective velocities by the geostrophic relations, we have,

$$\eta_1 = \frac{f_0}{g}\frac{\Psi_1}{\rho_1}$$

and

$$\eta_2 = \frac{f_0}{g}\frac{(\Psi_2 - \Psi_1)}{(\rho_2 - \rho_1)}. \tag{6}$$

On substituting for u_α and, η_1 and η_2 in eq. (4), we obtain, the potential vorticity equations,

$$\left(\rho_1 \frac{\partial}{\partial t} - \frac{\partial \Psi_1}{\partial y}\frac{\partial}{\partial x} + \frac{\partial \Psi_1}{\partial x}\frac{\partial}{\partial y}\right)$$
$$\times (\rho_1 \beta y + \nabla^2 \Psi_1 - F'\Psi_1 + F_1(\Psi_2 - \Psi_1)) = 0,$$
$$\left(\rho_2 \frac{\partial}{\partial t} - \frac{\partial \Psi_2}{\partial y}\frac{\partial}{\partial x} + \frac{\partial \Psi_2}{\partial x}\frac{\partial}{\partial y}\right)$$
$$\times (\rho_2 \beta_2 y + \nabla^2 \Psi_2 - F_2(\Psi_2 - \Psi_1)) = 0, \tag{7}$$

where

$$F_1 = \frac{f_0^2}{gH_1}\left(\frac{\rho_1}{\rho_2 - \rho_1}\right), \qquad F_2 = \frac{f_0^2}{gH_2}\left(\frac{\rho_2}{\rho_2 - \rho_1}\right),$$

$$F' = \frac{f_0^2}{gH_1},$$

and it has been assumed that,

$$\frac{\partial b}{\partial x} = 0, \qquad \frac{\partial b}{\partial y} = s,$$

where s is a constant bottom slope directed along Oy, such that $\beta_2 = \beta + f_0 s/H_2$.

The stability of this quasi-geostrophic system will be considered in the usual manner by supposing the existence of a zonal mean flow in each layer on which is superimposed a zonally propagating perturbation, i.e.,

$$\Psi_1 = -\rho_1 U_1 y + \Phi_1 e^{ik(x-ct)},$$

$$\Psi_2 = -\rho_2 U_2 y + \Phi_2 e^{ik(x-ct)}, \tag{8}$$

in which U_α are the zonal mean velocities, and Φ_α are mass streamfunctions for the perturbation ($|\Phi_\alpha| \ll |\Psi_\alpha|$) of wavenumber, k, and $c = c_r + ic_i$ in which c_r is the wavespeed, and if $c_i > 0$, the perturbation grows with time. The coupled model depends on three independent parameters (F_1, F_2 and F') of dimension (L^{-2}) which are inverse-squared Rossby radii of deformation for the system (cf. Section 3).

On substituting eqs. (8) in eq. (7) we obtain,

$$(\Phi_2 - \Phi_1) + \Phi_1\left(-\frac{k^2 + F'}{F_1} - \frac{P_1}{F_1(c - U_1)}\right) = 0, \tag{9}$$

$$-(\Phi_2 - \Phi_1) + \Phi_2\left(-\frac{k^2}{F_2} - \frac{P_2}{F_2(c - U_2)}\right) = 0, \tag{10}$$

where

$$P_1 = \beta + \frac{F_1(\rho_1 U_1 - \rho_2 U_2)}{\rho_1},$$

and

$$P_2 = \beta_2 - \frac{F_2(\rho_1 U_1 - \rho_2 U_2)}{\rho_2} \tag{11}$$

are the potential vorticities of the layers. Eqs. (9) and (10) can be treated in an identical manner to the small density contrast approximation equations to obtain the necessary conditions for instability (Pedlosky, 1964), and yield,

$$\frac{P_1}{F_1}\Delta U > 0, \qquad \frac{P_2}{F_2}\Delta U < 0, \tag{12}$$

where $\Delta U = U_1 - U_2$.

For the air-sea system, since usually $|U_2| >$

$(\rho_1/\rho_2)\,|U_1|$, the first inequality reduces approximately to the form,

$$\left(\frac{\beta}{F_1} - \frac{\rho_2}{\rho_1} U_2\right) \Delta U > 0,$$

which for all realistic conditions yields, $\Delta U > 0$. Hence, normally westerly winds would permit instability.

Similarly, the second inequality would be satisfied if,

$$\frac{\beta_2}{F_1} + \frac{H_1}{H_2}\frac{\rho_2}{\rho_1} U_2 < 0$$

and order of magnitude reasoning (assuming that H_2 is the depth of the oceanic layer) indicates that this inequality reduces to $\beta_2 < 0$ which is satisfied if,

$$\beta + \frac{f_0 s}{H_2} < 0.$$

In words, the necessary conditions for instability are normally satisfied for westerly winds, and an oceanic mixed layer which shallows towards the equator with a slope $|s| > \beta H_2/|f_0|$; the critical slope (at which $P_2 = 0$) being typically of magnitude 10^{-5}, which is commonly exceeded in oceanic data.

3. The instability analysis

We seek now the most rapidly growing waves in relation to the upper layer parameters U_1 and H_1, with the high density contrast assumption that $\rho_1/\rho_2 \ll 1$. The analysis is analogous to that of Gill et al. (1974) for a two layer ocean.

The characteristic equation derived from eqs. (9) and (10) is,

$$\begin{aligned} &c'^2[(k^2 + F_1 + F')(k^2 + F_2) - F_1 F_2] \\ &\quad + c'[\Delta U((k^2 + F_1 + F')(k^2 + F_2) - F_1 F_2) \\ &\quad + P_1(k^2 + F_2) + P_2(k^2 + F_1 + F')] \\ &\quad + P_1 P_2 + \Delta U P_1 (k^2 + F_1) = 0, \end{aligned} \tag{13}$$

where $c' = c - U$.

For equal roots with $P_2 = 0$ (cf. Section 2), eq. (13) yields the condition,

$$(k^2 - F_1 + F')(k^2 + F_2) - F_1 F_2 = \frac{P_1}{\Delta U}(k^2 + F_2)$$

of which the solution is,

$$k_0^2 = \frac{1}{2}\left(\frac{F_2 H}{H_1} - \frac{P_1}{\Delta U}\right) \times \left\{ -1 + \left(1 + \frac{4F_2((P_1/\Delta U) - F')}{((F_2 H/H_1) - (P_1/\Delta U))^2}\right)^{1/2} \right\}; \tag{14}$$

$$\frac{F_2 H}{H_1} > \frac{P_1}{\Delta U} > F',$$

where k_0 is the neutral wavenumber, and $H = H_1 + H_2$. At k_0 from eq. (11),

$$\Delta U = \frac{\beta_2 + F'(H_1/H_2)\,U_1}{F_2}. \tag{15}$$

We illustrate the neutral solution using reference parameters appropriate to an air-sea coupled system which consists of a barotropic atmosphere above an ocean mixed layer, namely,

$H_1 = 1000$ m, $U_1 = 10\ \mathrm{m\,s^{-1}}$, $H_2 = 200$ m,

$\rho_1 = 1.2\ \mathrm{kg\,m^{-3}}$, $\rho_2 = 1028\ \mathrm{kg\,m^{-3}}$,

$\beta = 2 \cdot 10^{-11}\ \mathrm{m^{-1}\,s^{-1}}$, $f_0 = 10^{-4}\ \mathrm{s^{-1}}$,

and define also the non-dimensional mixed layer bottom slope,

$$\theta = -\frac{f_0 s}{H_2 \beta}, \tag{16}$$

in which, for the reference parameters, $H_2\beta/f_0 = 4 \cdot 10^{-5}$.

Fig. 2 indicates the important result that the instability wavelength, $\lambda_0 = 2\pi/k_0$, and the corresponding bottom slope, s_0, are almost independent of the ocean current speed (U_2). Over a range of ± 1 knot, the neutral mixed layer slope varies only by $\pm 10\%$, and the neutral wavelength by $\pm 2\%$.

In the following discussion of the growth rates of the unstable waves, accordingly, it will be sufficient to illustrate the behaviour of the solutions, for

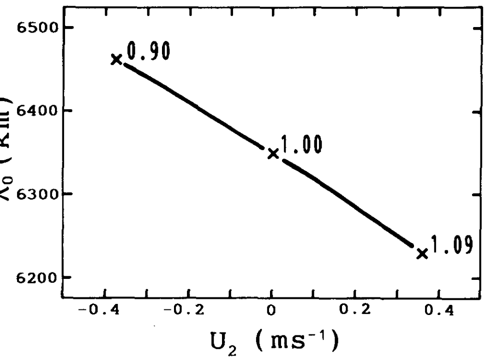

Fig. 2. The dependence of non-dimensional mixed layer slope (θ) on the neutral wavelength (λ_0) and the ocean current (U_2) for the reference parameters.

$U_2 = 0$ only, thus removing one physical variable from the system.

On defining a time constant for the growth of the unstable waves (e-folding time),

$$\tau = 1/kc_i, \tag{17}$$

we now seek the complex roots of eq. (13) for a series of non-dimensional bottom slopes, θ. Fig. 3a shows the result of this calculation for the reference parameters (and $U_2 = 0$). As anticipated from Section 2, unstable waves are found for all $\theta > 1$, the system being neutrally stable at $\theta = 1$ (Fig. 2). The most unstable wave has a growth rate (τ) of 98 days, a wavelength (λ_c) $\sim$ 3700 km, and occurs on a bottom slope of $-1.2 \cdot 10^{-4}$($\theta \sim 3$).

For each $\theta > 1$, there exists a *small* range of wavelengths which are unstable (Fig. 3b). The largest range of ± 75 km, occurs for $\theta \sim 2$.

An alternate presentation of the solutions (Fig. 4) illustrates the instability envelope in θ/k space, which is applicable in an ocean of the reference mixed layer depth $H_2 = 200$ m, and $U_2 = 0$ for the reference atmospheric parameters.

The next generalisation is to examine the dependence of the instability on H_2. This is achieved by locating the maximum growth rate for each, k, using the condition

$$\frac{\partial \tau}{\partial \theta} = 0 \tag{18}$$

as illustrated in Fig. 4, and leads to the solution of a cubic equation (an apparently equivalent procedure using the condition, $\partial \tau / \partial k = 0$, however leads to a sixth order equation).

The cubic equation is easily shown to be,

$$\Delta U v^3 + F_2\left(\frac{gs}{f_0}\left(1 - \frac{\rho_1}{\rho_2}\right) + \left(1 + \frac{H_2}{H_1}\right)\left(U_2 - \frac{\rho_1}{\rho_2} U_1\right) + \left(1 - \frac{H_2}{H_1}\right)\Delta U\right) v^2 - F_2\left(F_1 \Delta U + P_1\left(1 - \frac{H_2}{H_1}\right)\right) v + 2P_1 F_1 F_2 = 0, \tag{19}$$

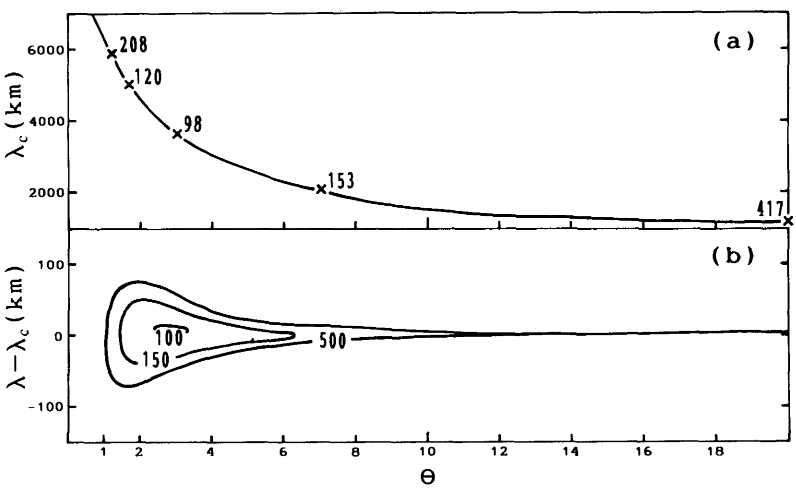

Fig. 3. (a) The dependence of the e-folding time (τ: days) of the most unstable wave on wavelength (λ_c) and non-dimensional mixed layer slope (θ). (b) The variation of e-folding time (τ: days) on the wavelength departure ($\lambda - \lambda_c$) and the non-dimensional mixed layer slope (θ) for zero ocean current ($U_2 = 0$) and the reference parameters.

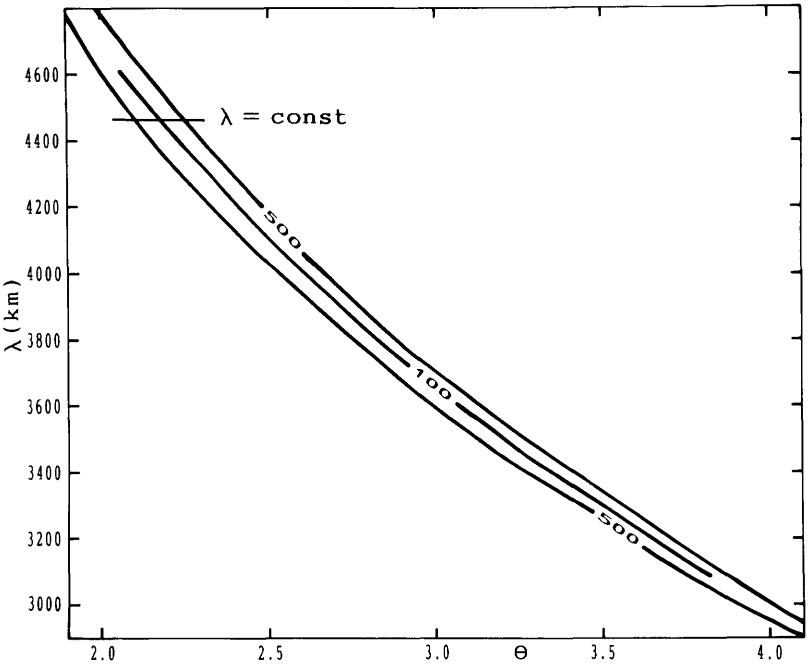

Fig. 4. The variation of e-folding time (τ: days) on wavelength (λ) and non-dimensional mixed layer slope (θ) for zero ocean current ($U_2 = 0$) and the reference parameters, showing the procedure for determining the minimum e-folding time.

where $v = k_c^2 + F_2(H_2/H_1)$, and k_c is the wavenumber of the most unstable wave.

Solutions of eq. (19) for the wavelength and the corresponding growth rate of the most unstable wave can be displayed in H_2/s space. (Figs. 5a and 5b). The $H_2 = 200$ m transect represents the solution shown in Figs. 3a and 3b, with a similar representation for other values of H_2. Fig. 5 indicates however that the wavelengths and growth rates of the most unstable wave are *not* strongly dependent on H_2 for all realistic mixed layer depths, and also that the solution is regular in the limit of $H_2 \to 0$. In this limit $F_2 \to \infty$ and eq. (19) simplifies to the quadratic equation,

$$v^2(1-\varepsilon^2)\left[\frac{gs}{f_0} + U_1\right] - v\left[\beta_1 + \frac{2F'\varepsilon^2}{1-\varepsilon^2}\Delta U\right] + 2\left(\beta_1 + \frac{F'\varepsilon^2}{1-\varepsilon^2}\Delta U\right)\frac{F'\varepsilon^2}{1-\varepsilon^2} = 0, \qquad (20)$$

where

$$\beta_1 = \beta - F'U_2, \qquad \varepsilon = (\rho_1/\rho_2)^{1/2},$$

$$v = k_c^2 + F'\left(\frac{1}{1-\varepsilon^2}\right),$$

of which the solution to $O(\varepsilon^2)$ is,

$$v = \frac{1}{(gs/f_0) + U_1}\left[\beta_1 + \varepsilon^2\left(\beta_1 - 2F'\left(\frac{gs}{f_0} + U_2\right)\right)\right]$$

from which to $O(1)$, we have,

$$k_c^2 = \frac{\beta_1}{(gs/f_0) + U_1} - F'. \qquad (21)$$

For the limit $F_2 \to \infty$, the characteristic equation (eq. (13)) reduces to the form,

$$\left(v - \frac{F'\varepsilon^2}{1-\varepsilon^2}\right)c'^2 + \left(v(1-\varepsilon^2)\left(U_1 + \frac{gs}{f_0}\right) + \beta_1\right)c' + (1-\varepsilon^2)\left(U_1 + \frac{gs}{f_0}\right)\left(\beta_1 + \frac{F'\varepsilon^2}{1-\varepsilon^2}\Delta U\right) = 0, \qquad (22)$$

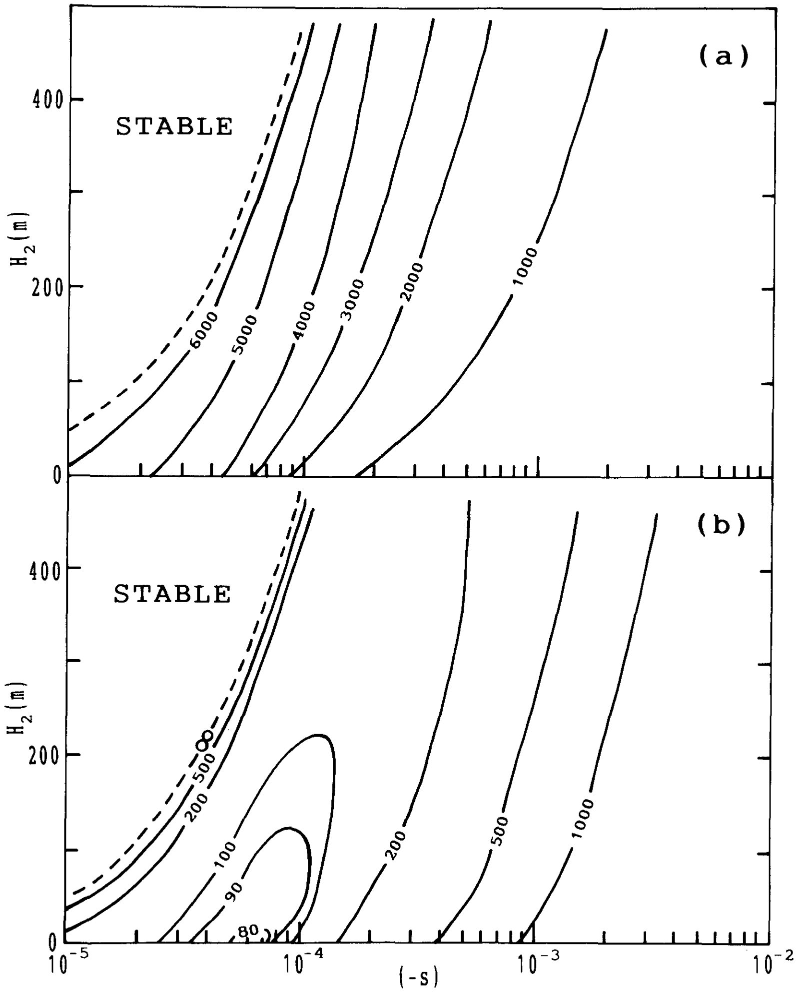

Fig. 5. (a) The dependence of the wavelength (λ_c: km) of the most unstable wave on mixed layer depth (H_2) and slope ($-s$). (b) The dependence of the e-folding time (τ: days) of the most unstable wave on mixed layer depth (H_2) and slope ($-s$) for a zero ocean current, $U_2 = 0$, and the reference parameters. The dashed line indicates the limit of the unstable region.

of which to O(ε), the solution is,

$$c' = -\left(U_1 + \frac{gs}{f_0}\right)\left\{1 \pm i\varepsilon\left(\frac{-F'(U_2 + (gs/f_0))}{\beta_1}\right)^{1/2}\right\},$$

$$U_2 + \frac{gs}{f_0} < 0. \tag{23}$$

On substituting for k and c_i in eq. (17) from eqs. (21) and (23) and using the maximum growth rate condition (eq. (8)), it is easily shown that

$$\frac{gs}{f_0} = -\left[U_1 - \frac{1}{3}\left(\Delta U + \frac{\beta_1}{F'}\right) + \frac{1}{3}\left(\left(\frac{\beta_1}{F'} + \Delta U\right)^2 - \frac{3\beta_1}{F'}\Delta U\right)^{1/2}\right]. \tag{24}$$

Hence, on substituting for (gs/f_0) in eqs. (17), (21), (23), we obtain explicit expressions for λ_c, c_r, T $(=\lambda_c/c_r)$ and τ in terms of the atmospheric parameters H_1 and U_1. Fig. 6 shows the resulting solutions with $U_2=0$.

It is apparent that a family of unstable waves exists with e-folding times (τ) of order 100 days, similar to that for oceanic eddies (Gill et al., 1974).

The ratio of the mass streamfunctions in each fluid for the most unstable wave is,

$$\frac{\Phi_1}{\Phi_2}=\frac{i\varepsilon F'^{1/2}(U_1+(gs/f_0))}{(-(U_2+(gs/f_0)))^{1/2}\,\beta_1^{1/2}}, \tag{25}$$

which occurs with a kinetic energy ratio of

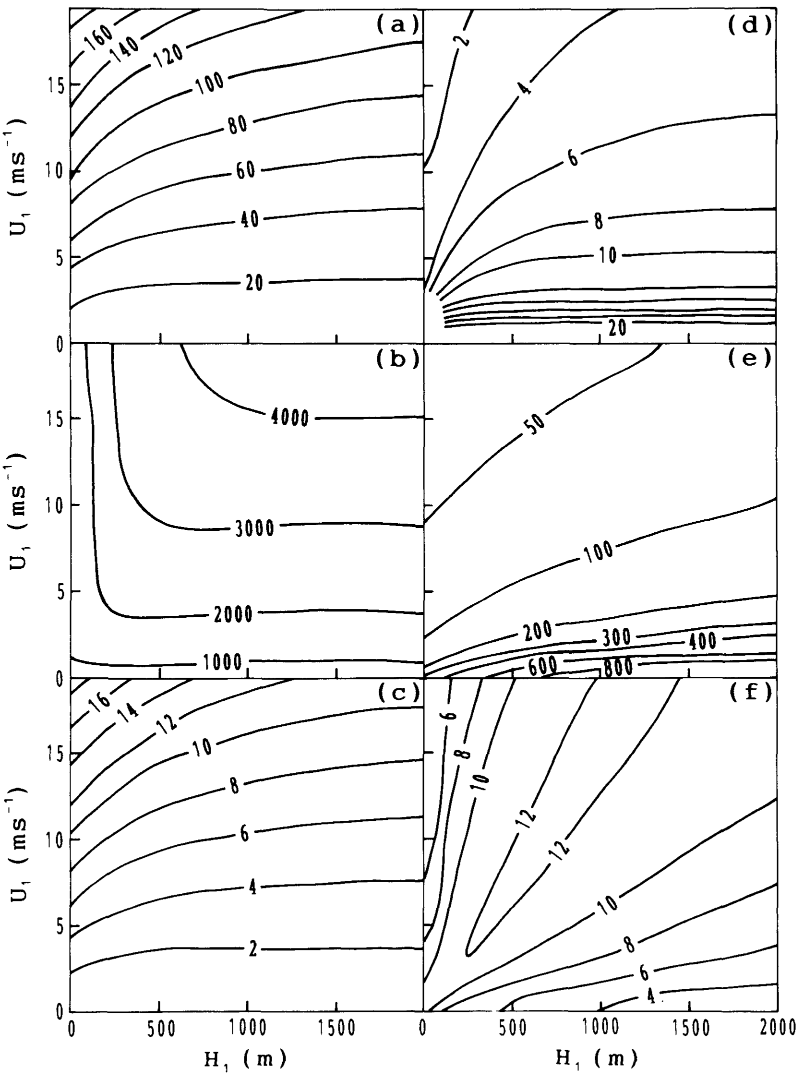

Fig. 6. Properties of the most unstable wave as a function of atmospheric depth (H_1) and velocity (U_1) for zero ocean current ($U_2=0$) and mixed layer depth $H_2\to0$. (a) Mixed layer slope ($-s\times10^6$). (b) Wavelength (λ_c: km). (c) Wavespeed (c_1: m s^{-1}). (d) Period (T: days). (e) e-folding time (τ: days). (f) Volume streamfunction ratio $|\Phi_1/\Phi_2\varepsilon^2|$.

$(\Phi_1/\varepsilon\Phi_2)^2$, and a velocity ratio of $(\Phi_1/\Phi_2\varepsilon^2)$. Fig. 6f shows that in the most unstable wave oceanic velocities are about one tenth of the atmospheric velocities, but oceanic kinetic energy/unit depth is ten times atmospheric kinetic energy/unit depth or, alternatively, (since in the real ocean $H_2 \sim 0.1 H_1$) the kinetic energy is approximately equally partitioned between the two fluids.

For the perturbation, on using eq. (6), the atmospheric pressure anomaly,

$$p'_a = f_0 \Phi_1,$$

and the pressure anomaly in the mixed layer,

$$p'_0 = f_0 \Phi_2. \tag{26}$$

Hence, since $\Phi_1/\Phi_2 \sim 0.01$, the pressure anomalies in the mixed layer are much greater than in the atmosphere.

From eq. (23), the wavespeed of the growing wave,

$$c_r = -\frac{gs}{f_0} \tag{27}$$

which (to O(1)) is independent of the ocean current.

In the atmosphere, c_r is due to a divergent barotropic wave steered by the wind velocity, thus,

$$c_r = U_1 - \frac{\beta_1}{k_c^2 + F'}, \tag{28}$$

which, from eq. (21), reduces to $-(gs/f_0)$. Note that the only effect of the ocean is through a small change in the potential vorticity due to the slope on the ocean surface,

$$\beta_1 = \beta - F'U_2 \sim \beta + \frac{f_0}{H_1}\frac{\partial \eta_2}{\partial y},$$

where

$$\left|\frac{\beta_1 - \beta}{\beta}\right| \sim 0.01.$$

Fig. 7 shows the growth rates for the most unstable wave in the presence of an ocean current, $U_2 = 0.5$ m s^{-1}; the variation τ with H_1 and U_1 is

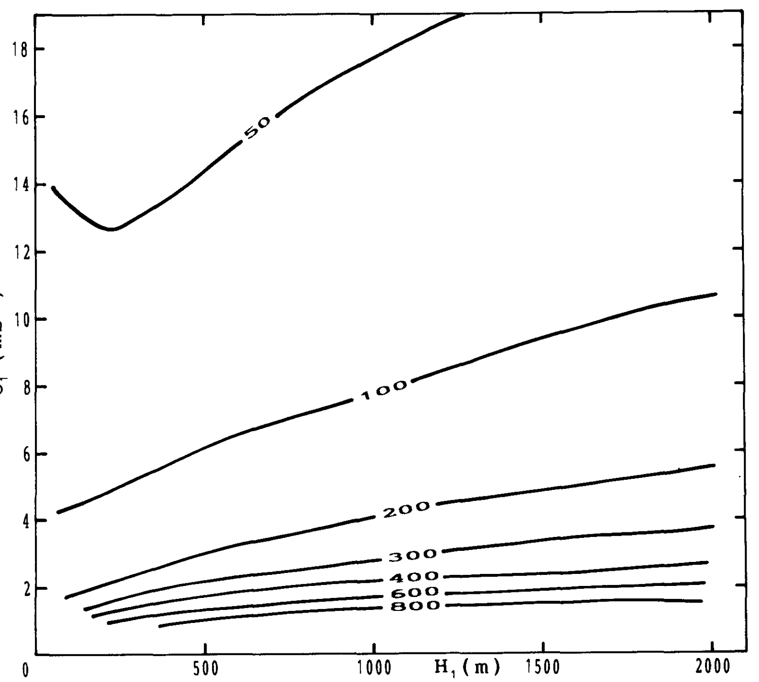

Fig. 7. The e-folding time (τ: days) of the most unstable wave as a function of the atmospheric depth (H_1) and velocity (U_1) for an ocean current ($U_2 = 0.5$ m s^{-1}) and a mixed layer depth ($H_2 \to 0$) for the reference parameters.

almost identical to that occurring in a motionless ocean (Fig. 7), except for $U_1 \sim U_2$. In the ocean, c_r is due to a mixed layer "topographic wave",

$$c_r = -\frac{\beta_2}{F_2 + k_c^2} \sim -\frac{gs}{f_0}, \tag{29}$$

and, since $F_2 \gg k_c^2$, the oceanic response is non-dispersive.

In this system, the oceanic mixed layer is coupled with the atmosphere in a response (cf. Section 4) which is independent of the baroclinic interactions within the water column. Eq. (25) indicates that the atmospheric wave leads the oceanic wave by $\pi/2$ as illustrated in Fig. 8 for the southern hemisphere. The behaviour of the solution can be generalised finally for the limit of $U_2 = 0$ and $H_1 \to \infty$, such that $F' \to 0$.

In this limit, the properties of the most unstable wave are,

$$s = -\frac{1}{2}\frac{f_0}{g} U_1, \qquad \lambda = \pi\left(\frac{2U_1}{\beta}\right)^{1/2},$$

$$\tau = \frac{2(gH_1)^{1/2}}{\varepsilon U_1 f_0}, \qquad c_r = \tfrac{1}{2} U_1$$

$$\frac{\Phi_1}{\Phi_2} = i\left(\frac{U_1}{2\beta g H_1}\right)^{1/2} \varepsilon f_0, \qquad T = 2\pi\left(\frac{2}{U_1 \beta}\right)^{1/2}. \tag{30}$$

Table 1 indicates that the errors in using these

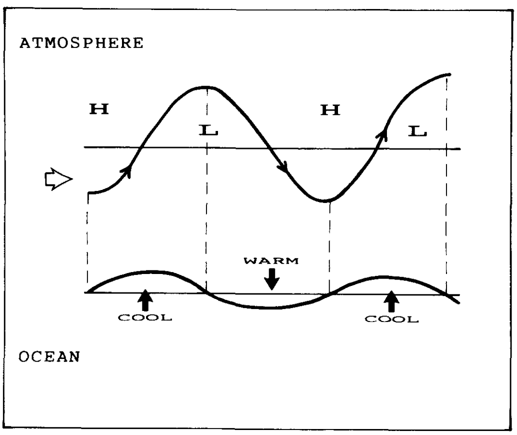

Fig. 8. Cartoon of the most unstable coupled wave in the southern hemisphere.

Table 1. *Comparison between the exact solution and eq. (30) of the most unstable wave with the parameters $U_1 = 10\ m\ s^{-1}$, $U_2 = 0\ m\ s^{-1}$, $H_1 = 1000\ m$, $\rho_1 = 1.2\ kg\ m^{-3}$, $\rho_2 = 1028\ kg\ m^{-3}$, $\beta = 2 \cdot 10^{-11}\ m^{-1}\ s^{-1}$, $f_0 = 10^{-4}\ s^{-1}$ and $H_2 \to 0$*

	Exact solution	from eq. (30)
s	$-5.9 \cdot 10^{-5}$	$-5.1 \cdot 10^{-5}$
τ (days)	77	58
λ (km)	3250	3140
c_r (ms^{-1})	5.8	5.0
$\frac{1}{\varepsilon^2}\frac{\Phi_1}{\Phi_2}$	11.6 i	14.8 i
T (days)	6.5	6.3

results for $H_1 = 1000$ m and $U_1 = 10\ \text{m s}^{-1}$, are not generally large. The limiting solution (eq. (30)) is independent of F_2 and F' and governed by $F_1 \sim f_0^2 \varepsilon^2 / gH_1$. The "barocopular Rossby radius of deformation" which corresponds with F_1 is

$$D_c = (gH_1)^{1/2} / f_0 \varepsilon,$$

and for the parameters of Table 1, $D_c \sim 30 \cdot 10^3$ km, is of World dimension.

In the limiting solution (eq. (30)) for the high density contrast situation, F_1 is the *smallest* of the three parameters in eq. (7). For the corresponding limiting solution in the low density contrast situation, the governing parameter is the *largest* of the three parameters, e.g., baroclinic instability in the ocean is characterised by F_1 and the baroclinic Rossby radius of deformation, $D_0 = (g'H_1)^{1/2}/f_0$,

Table 2. *Properties of the most unstable waves with $U_1 = 10\ m\ s^{-1}$ (50° S) and $U_1 = 2\ m\ s^{-1}$ (35° S) obtained from the exact solution with parameters other than U_1 identical with Table 1*

	50° S	35° S
U_1 (m s^{-1})	10	2
s	$-6 \cdot 10^{-5}$	$-1 \cdot 10^{-5}$
τ (days)	80	340
λ (km)	3300	1400
c_r (m s^{-1})	6	1
$\frac{1}{\varepsilon^2}\frac{\Phi_1}{\Phi_2}$	12 i	6 i
T (days)	7	16

where $g' = g(\rho_2 - \rho_1)/\rho$ and $(\rho_2 - \rho_1)/\rho \ll 1$ in which $\rho \sim \rho_1 \sim \rho_2$, and in the atmosphere, by F_2 with a baroclinic Rossby radius of deformation. $D_a = (g'H_2)^{1/2}/f_0$. The baroclinic Rossby radii (D_0 and D_a) both have scales much less than the scale of the atmosphere-ocean system, but the barocopular Rossby radius (D_c) appears to be of similar scale.

4. Discussion

The basic transformation in this analysis has been to incorporate the mixed layer into the atmosphere rather than the oceanic dynamical system. This change of reference has indicated the existence of a family of coupled air-sea modes unsuspected in classical analyses.

The importance of these modes is determined by the integrity of the mixed layer as a wave guide independent of the deep ocean. Our simple two-layer analysis cannot address this question, which can only be investigated using a model which correctly represents mixed layer formation, and exchange of momentum at the base. The results of such a model would determine the strength of the anomalies to be expected by the barocoupling process.

These barocoupled anomalies would manifest themselves in three ways: (a) as an interseasonal atmospheric pressure signal; (b) as a current system confined to the mixed layer; (c) as a pressure signal transmitted to the deep ocean below the mixed layer.

These interrelated phenomena are discussed below. Firstly however we examine mixed layer depths in the World Ocean, bearing in mind that there is some sensitivity in establishing the depth contours, since it is not sufficient generally to use a temperature based criterion only, and the coverage of near surface salinity profiles is not adequate. The March and September charts of (Levitus 1982), however although relatively noisy, clearly indicate mixed layer depths which shallow towards the Equator under the westerly winds. In the southern ocean between 40° S and 50° S, we estimate an average slope of $-5 \cdot 10^{-5}$ in March, and -10^{-4} in September. These estimates are remarkably similar to the theoretical slope range in Table 2. A similar behaviour is observed in the westerly wind belts of the northern hemisphere, but throughout the world ocean, almost constant mixed layer depths occur under the trade winds.

This pattern strongly suggests a barocoupling response for the air-sea system, in which the thermodynamics of the coupled system has a sufficient number of degrees of freedom to ubiquitously generate the requisite mixed layer variability under the westerly wind belts.

Table 2 shows the properties of the most unstable wave for a reference atmospheric depth, $H_1 = 1000$ m and two zonal atmospheric velocities $U_1 = 10 \text{ m s}^{-1}$ and $U_1 = 2 \text{ m s}^{-1}$, which in the southern hemisphere occur at approximately latitudes 50° S and 35° S. Some deductions are as follows:

At 50° S, the most unstable wave would circle the World in about 40 days, but at 35° S, the progression is much slower, of order 100 km/day. Over the same latitude range, the wavelength decreases from about 3000 km to 1500 km (the form of the coupled wave over these time and space scales is shown in Fig. 8). The e-folding time (τ) at all latitudes is of seasonal time scale. Hence, during the march of the seasons, characterized by a mean zonal wind field, $U_1(y, t)$, one would expect the generation of a continuum of waves of varying wavelengths and wavespeeds, which would modulate the atmospheric interseasonal dynamics, particularly in the maritime environment of the Southern Hemisphere. In the ocean however, the nondispersive response indicates that the passage of the waves would oscillate features meridionally without change of form. The implication is that synoptic events are steered by a wind field which can be predicted (in principle) from a knowledge of the mixed layer topography and wind field of a few months earlier. In short, weather patterns have a seasonal memory.

The meridional perturbation velocities in the two fluids scale approximately in the ratio 1:10 (Table 2), such that a particle speed of 1 m s^{-1} in the atmosphere corresponds with a particular speed of 10 cm s^{-1} in the ocean.

At 50° S, maximum meridional wind anomalies of 1 m s^{-1} would occur for atmospheric pressure anomalies (p'_a) of amplitude of about 0.6 hPa, and would give rise to north-south excursions during the passage of the wave of 180 km in the atmosphere, and 15 km in the ocean. Similarly, at 35° S, the respective magnitudes would be 0.3 hPa, 450 km and 70 km. The corresponding amplitudes of the pressure anomaly (p'_0) in the mixed layer for 50°S and 35°S respectively, using eq. (26), are 45 hPa and 35 hPa, which would correspond with sea level amplitudes of ~0.4 m.

We suggest that the incorporation of these ideas into a coupled general circulation model may be rewarding, especially in relation to interseasonal climate variability in the southern hemisphere.

REFERENCES

Gill, A. E., Green, J. S. A. and Simmons, A. J. 1974. Energy partition in the large-scale ocean circulation and the production of mid-ocean eddies. *Deep-Sea Res. 21*, 499–528.

Levitus, S. 1982. Climatological atlas of the World Ocean. *NOAA Professional Pap. 13*, U.S. Dept. Comm. 173 pp.

Pedlosky, J. 1964. The stability of currents in the atmosphere and the ocean: Part I. *J. Atmos. Sci. 21*, 201–219.